

New explanation of the strange baryon rapidity distributions in ultra-relativistic nucleus-nucleus collisions.

J. A. Casado ¹

Department of Physics and Astronomy,
University of Manchester,
Manchester, M13 9PL, England.

Abstract

A model of multiparticle production in hadronic collisions at ultra-relativistic energies, based on the assumption of independent string fragmentation, reproduces the rapidity spectra of Λ and $\bar{\Lambda}$ in sulphur-sulphur collisions reported by the NA35 Collaboration. This is achieved after a reconsideration of the intermediate multi-string states and the structure of the diquarks. Nuclear stopping power is also studied through the computation of the $p - \bar{p}$ rapidity spectra.

¹ E-mail: casado@a13.ph.man.ac.uk

1 Introduction

Strange particle production in heavy ion collisions is a subject of great interest since it may provide evidences of the formation of a new state of matter: the quark-gluon plasma (QGP). The tantalizing pursuit of this discovery is the justification for the efforts being made to carry out the heavy-ions collision experiments that have taken place at the AGS and CERN-SPS, and to plan new ones for future facilities. A phase transition between normal nuclear matter to a deconfined phase has been predicted long ago^[1, 2] to occur at very high temperatures and densities. For the time being, the properties of the QGP have not being clearly stabilised, neither the order of the phase transition between the two states. This makes the problem of recognizing the formation of QGP, if it happens, particularly difficult, more so since we have to rely on indirect clues to its detection. Several signatures have being proposed for this purpose that may deliver circumstantial evidences of the formation of quark matter (for an up-to-date review on the subject with a complete list of references, see [3]). The strange mesons, baryons and antibaryons production has been predicted to be greatly enhanced in the presence of QGP as compared to the case when there are only standard hadron matter^[4, 5]. Also the study of the stopping power may help to uncover the presence of the deconfined phase: a rapid change in the shape of the rapidity baryon distributions with increasing incident beam energy is thought to be a clear signal for new degrees of freedom^[6].

An additional problem is caused by the lack of a full description of the confined phase, which constitutes the background to the events in which QGP may have been formed. *Enhanced strange particle production* is a meaningless expression unless we can find out what strange particle production must be expected from an ordinary ion-ion collision event. We can not extract this information from QCD since we do not know how to apply this theory when the effective coupling constant is not small. This is also the ultimate cause of the lacunae in our understanding of the QGP properties and of the order of the phase transition mentioned in the above paragraph. We have to rely on phenomenological models to fill this gap. The Dual Parton Model (DPM)^[7] and the Quark Gluon String Model (QGSM)^[8, 9] have been very successful in describing many features of hadron-hadron, hadron-nucleus and nucleus-nucleus collisions. Nevertheless, they were not able to reproduce^[10] the rapidity distributions of Λ and $\bar{\Lambda}$ hyperons, as well as proton minus antiprotons ($p - \bar{p}$), in central sulphur-sulphur collisions measured by the NA35 Collaboration^[11, 12]. The idea that the onset of the deconfinement phase transition may be at the origin of this disagreement is very appealing. However, we must carefully explore any other possible explanation of these data before admitting that eventuality. The NA35 data show a large production of Λ 's in the fragmentation as well as in the central region. It is very difficult to understand why the formation of QGP in a collision between identical nuclei should contribute so largely to the borders of the accessible phase space. This can not obviously be due to QGP formation as it should mainly affect the hadron spectra in the central rapidity region. Besides, QGP formation in this experiments, involving relatively light nuclei, would come as a striking surprise. The energy densities currently available at the AGS and CERN-SPS of $0.5-10 \text{ GeV}/\text{fm}^2$ correspond to temperatures between 100 and 200 MeV^[13], for which the effective coupling constant of QCD is not less than 1, and we should not be expecting a deconfinement phase transition to occur. This also should encourage us to look for conventional explanations to the phenomena observed in heavy nucleus collisions that have not been understood so far.

Strangeness enhancement is also present in pp interactions. The ratio K/π increases both with the energy of the collision and with the multiplicity^[14]. It has also been observed an increase of the ratio $\bar{\Lambda}/\bar{p}$ in pp collisions as the centre-of-mass energy increases from 20 GeV to 1800 GeV^[15]. Again, the NA35 Collaboration also reported that strangeness is enhanced between pp and pS collisions^[11]. At the same time, the average number of collisions per participant nucleon increases between pp and pA collisions as well as between pA and central AB collisions. This increase is also correlated with an increase of the multiplicity of secondaries. According to the DPM and the QGSM, the extra particles are produced by the fragmentation of strings that have sea quarks at their ends. As this mechanism on its own failed to reproduce the observed enhancement of Λ and $\bar{\Lambda}$ in central SS collisions, additional sources of this increase have been explored.

Diquark-antidiquark pairs from the nucleon sea have been introduced^[16, 17, 18]. This model predicts, contrary to the experimental evidence, the same increase in the absolute value of strange baryons and antibaryons. It may also be worth mentioning that this mechanism is very similar in its formulation and its results to the, so called, string fusion model of ref. [19]. In reference [10] the problem is treated considering final state interactions of co-moving pions and nucleons of the type $\pi + N \rightarrow K + \Lambda$. This approach is not convincing since it contains the unrealistic assumption that all baryons are created instantaneously at the beginning of the collision so the secondary collisions can take place.

What the data on strange baryon production of the NA35 Collaboration may actually be suggesting is that we may be missing an important piece in our understanding of the nucleon-nucleon rescattering. I devote this paper to reconsider how the valence and sea quarks take part in the formation of the ends of strings. I will show that, by allowing the leading diquarks to be formed not only of valence quarks, a good understanding of the data in the fragmentation region is obtained. I also considered the net proton distribution, usually regarded as a measurement of the stopping power of nuclear matter. Data from the NA35 Collaboration shows a larger stopping than predicted. The model proposed here also gives better results for this particular problem.

There have been a couple of other mechanisms proposed that could contribute to the full explanation of the data. One of them^[20] assumes that diquarks can break up into two quarks, one of which can be slowed down along the string carrying the string junction (baryon number) and produces much slower baryons. The other^[21] consists in considering the possibility that the baryon number is not always carried by a diquark, or a quark as in the previous case, but by a non-perturbative configuration of gluon fields. Both have similar phenomenological implications as both mainly affect the centre of the rapidity space and can not account for what happens in the fragmentation region what is my major concern in this paper, in particular for the case of Λ production.

There are a number of other models that are also constructed around the idea of independent fragmentation of strings. The best known is the Lund-Fritiof model^[22]. Although the general assumptions are at first sight very similar to the ones in DPM and QGSM, the theoretical basis from which these models were developed are quite different and I will not refer to them in the rest of the paper.

In section 2 I discuss the theoretical basis of the paper and make a full description of the model. The next two sections deal with fits to pp data to obtain the value of some parameters of the model, and the results for nucleus-nucleus collision. The paper ends with the conclusions.

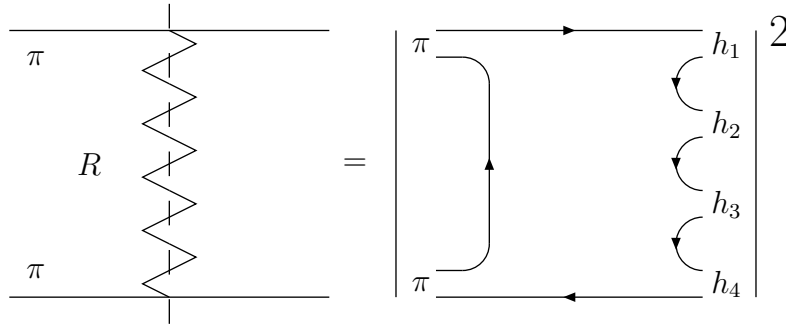


Figure 1: Representation of a cut reggeon and its relation with the planar diagram.

2 The Model

The independent-fragmentation string models, DPM and QGSM, were inspired by the developments of the Dual Topological Unitarization (DTU)^[23, 24, 25, 26, 27]. The amplitudes of high-energy hadronic collisions were formally written as an expansion in powers of $1/N_f$, where N_f is the number of flavours. Each term in the expansion can be associated with a diagram with a definite topology. The scheme was based on the S-matrix analysis and was closely related to the Regge Field Theory (RFT). The DTU program was reinforced when Veneziano^[28] established a conceptual link with QCD as he included in the series powers of $1/N_c$ ^[29, 30, 31], being N_c the number of colours. In this way, the whole series of the topological expansion formally includes all the terms of the perturbative QCD series ensuring unitarity.

The lowest order term (fig. 1) is the planar diagram connecting two colliding-hadron lines. It represent the exchange of an object that has the same quantum number of the Reggeon and can be identified with it. Unitarity requires the inclusion of all diagrams obtained by repeatedly multiplying the planar term by itself. The next order topology we have to consider is that of the cylinder that corresponds to the Pomeron (see fig. 2) as it only vacuum quantum numbers can be exchange in the elastic collision. Higher order terms can be obtained by combining the simplest topologies described above, and all of them have a one to one correspondence with Reggeon Field Theory (RFT) diagrams. Bearing in mind that we are interested in the high-energy regime, we make use of this correspondence to neglect terms containing the exchange of one or more reggeons: although they may be dominant in the topological expansion, their contribution decreases with the centre-of-mass energy squared s as $s^{\alpha_R(0)-1} \sim s^{-0.5}$ while the pomeron exchange subdiagrams behave like $s^{\alpha_P(0)-1} = s^\Delta$, where $\Delta \geq 0$.

This formal developments laid the foundation of phenomenological models that had to fill the conceptual gaps left by the theory. Both DPM and QGSM postulated that multiparticle production in hadronic collisions at ISR energies, take place in two definite steps. First, the hadrons split in two fragments that share the total momentum of the hadron according to the corresponding structure functions. One of the fragments belongs to the $\mathbf{3}$ representation of the $SU(3)$ colour group, a quark, and the other to the $\bar{\mathbf{3}}$ representation, an antiquark in the case of a meson or a diquark in the case of a baryon. Secondly, two colour strings are formed each one

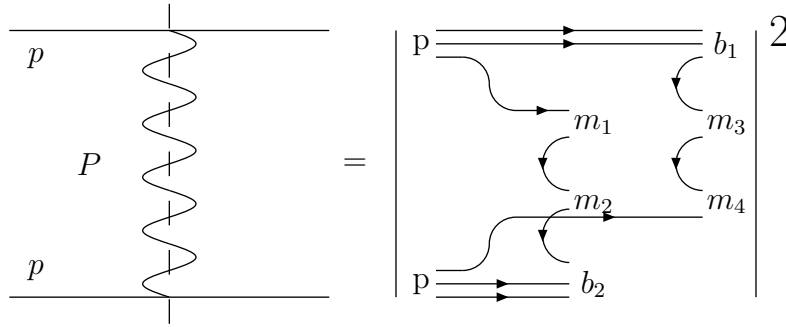


Figure 2: Diagrammatic representation of a cut pomeron and its relation with the cylinder diagram.

having a fragment of the 3 representation in one end from one of the hadrons, and another of the $\bar{3}$ representation, from the other hadron at the other end. These two strings decay into two chains of hadrons that form the final multiparticle state. The contribution of a string to the final state is given by the fragmentation functions that are, along with the structure functions, the other basic ingredient of the models.

When we move to higher energies, we have to introduce terms with more than two strings that correspond to diagrams with several cut pomerons. The probability weights of the different diagrams are given by the perturbative RFT that can be effectively described by a generalized eikonal model^[7]. Each cut pomeron add two chains of hadrons to the final state as the result of the decay of two more strings. The generalization of the models to hadron-nucleus and nucleus-nucleus collisions carries some similarities with this extrapolation to higher energies. In this case, multiple inelastic collision appears as a consequence of the rescattering of each nucleon by the nucleons on the other interacting nucleus. Again, for each additional inelastic collision we have to consider the fragmentation of two extra chains. The probability weights are given in this case by an external model like that of Glauber-Gribov, that reproduces the geometry of the collision.

Both DPM and QGSM assume that the diquarks at the end of the strings in hadronic collisions, are always made of valence quarks. So, in the case of a colliding proton, regardless of the number of cut pomerons in the collision, the diquark can only be of type (uu) or (ud) . The central point to this paper is the assumption that the sea quarks can be part of the diquark with the same probability as the valence quarks. It is still true that the diquark in a proton can only be of the types mentioned above when it suffers only one inelastic collision. But, when the number of cut pomerons is greater than one, we also have to consider diquarks of the type (dd) , (us) , (ds) and (ss) . The flavour content of the diquark depends on the flavour content of the hadron sea.

This assumption means the inclusion of terms of the topological expansion that are missing in the other independent strings fragmentation models. They correspond to diagrams where the cylinder (the pomeron) is linked to the colliding hadron through a $q^v \bar{q}^s$ or $\bar{q}^v q^s$ trajectory as depicted in fig. 3(b). For the incoming nucleon to interact with two nucleons of the target

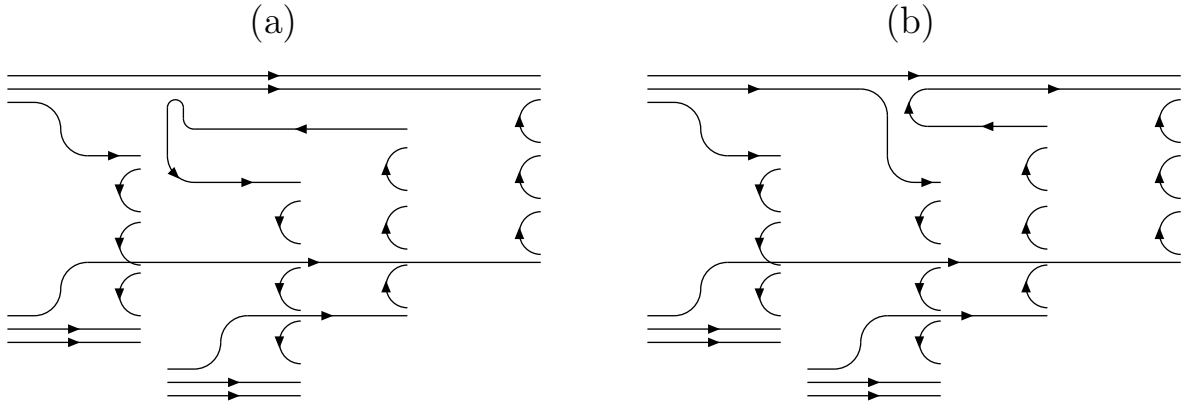


Figure 3: Two diagrams corresponding to inelastic collisions of a nucleon with two nucleons from the target. Diagram (a) is common to all models, while diagram (b) is one of the new components considered in this paper.

it is necessary that it appears in a virtual state composed of a baryon-like and a meson-like states. Then, the topology of the interaction can be depicted as the superposition of a baryon-nucleon and a meson-nucleon collisions. In other models, the baryon-like state could only be formed with the three valence quarks, and only meson-like states of the type $|u\bar{u}\rangle$, $|d\bar{d}\rangle$, etc, were considered. I am dropping this restriction only justified for high-mass intermediate states, where sea quark-antiquark pairs are created with large values of rapidity (> 1) respect to their parent hadron. Therefore, in a proton - nucleus collision we now have to include, besides $|p^* \pi^{0*}(\rho, \dots)\rangle$, states like $|\Lambda^* K^{+*}\rangle$ ².

These new components enhance the production of the strange baryons in the fragmentation region due to the contribution of strange diquark fragmentation. I consider a theory with only three flavours: u , d and s , and assume that the u and d contents of the sea are equal, while the s content is suppressed and represented by the parameter S .

$$S = \frac{2\bar{s}}{\bar{u} + \bar{d}} \quad . \quad (1)$$

SU(3) symmetry corresponds to a value $S = 1$. I take $S = 0.5$ that is compatible with several data analysis^[15, 32, 33]. In the rest of the paper, I will be using γ as the portion of strange sea-quarks over the total number of sea-quarks:

$$\gamma = \frac{\bar{s}}{\bar{u} + \bar{d} + \bar{s}} = \frac{S}{S + 2} \quad . \quad (2)$$

For the given value of S , $\gamma = 0.2$.

² *Baryon-like* and *meson-like*, as well as the asterisks, mean that they are not real baryons or meson since only the flavour content is considered and no attention is paid to other quantum numbers

2.1 Structure Functions

The only essential difference between the DPM and the QGSM comes from the way they postulate the structure functions for sea quarks and antiquarks. Only the leading behaviour at $x \rightarrow 0$ is retained in all cases, that has been called the *retardation* of the hadron fragments. In a collision in which there is only one cut pomeron, the retardation of a quark of flavour f depends on the intercept of the corresponding $q^f \bar{q}^f$ trajectory while for the diquark depends on the intercept of the corresponding $qq\bar{q}$ exotic trajectory. When dealing with nucleons, for these functions we have

$$f_{qv}(x) = x^{-\alpha_R}, \quad f_{qq}(x) = x^{\alpha_R(0) - 2\alpha_N(0)} \quad . \quad (3)$$

Where we have made use of the equation, valid in the planar approximation, $\alpha_{q^a q^b \bar{q}^c} + \alpha_{q^c \bar{q}^a} = 2\alpha_{q^a q^b q^c}$ and $\alpha_R(0)$ ($\alpha_N(0)$) is the zero intercept of the leading Regge (nucleon) trajectory.

When there are more than one cut pomeron, we need quarks and antiquarks from the sea to make up enough string ends. In the DPM, it is assumed that quark-antiquark pairs are formed as the result of the decay of a pomeron which has a retardation given by $1/x$. Following this line of reasoning DPM postulates that the retardation of a sea quark or sea antiquark is given by

$$f_{q^{sea}}^{(DPM)}(x) = \frac{1}{\sqrt{x^2 + (\mu^2/s)}} \quad . \quad (4)$$

Where μ is a parameter that sets a mass scale. QGSM postulates, on the other hand, that the retardations of the sea quarks and antiquarks have the same origin as that for valence quarks and, hence, are the same functions. I adopt this latest view in the present work. While there are no practical difference in terms of computational results at ISR energies, I find QGSM structure functions more coherent with the assumption I have made – sea-valence diquark symmetry. The mechanism considered in DPM to postulate the retardation functions, must be included in a treatment of the problem in which we sum over all possible RFT diagrams. For instance, in the case of two inelastic collisions, one term must correspond to a coupling between the hadron and the two cut pomerons mediated by the exchange of a pomeron (DPM) – PPP diagram, another one to the same coupling mediated by the exchange of a reggeon (QGSM)– PRP diagram. The corresponding relative weights for this kind of diagrams are not known and their computation is an open problem. The choice among neglecting one or the other constitutes a model assumption that can only be justified by the phenomenology^[34]. Yet, the eikonal approximation to RFT points that the PPP diagrams constitute the main contribution to high-mass intermediate states and eventually lead to the point-like quarks structure functions, while the PRP type of diagrams are the dominant terms for low-mass intermediate states^[35]. This idea allowed to understand the data from HERA on small-x behaviour of the structure functions^[36].

The PPP coupling does not allow the inclusion of diagrams of type 3(b). The extra sea quark-antiquark pairs, in collisions with more than one cut pomeron, are the result of the decay of an object with vacuum quantum numbers. Therefore, DPM only allows diagrams of type 3(a). This also explains why only valence diquarks contribute to the final state in DIS and hard hadron-hadron collisions. Then, as far as we are interested in the low- p_\perp regime, it seems most reasonable to adhere to QGSM view.

The s-quark, (us), (ds) and (ss) retardations are given by the following functions, where α_φ is the intercept of the φ trajectory and $\Delta\alpha = \alpha_R(0) - \alpha_\varphi(0)$.

$$\begin{aligned}
f_s(x) &= x^{\alpha_\varphi} \quad , \\
f_{us}(x) &= f_{ds}(x) = x^{\alpha_R(0)-2\alpha_N(0)+\Delta\alpha} \quad , \\
f_{ss}(x) &= x^{\alpha_R(0)-2\alpha_N(0)+2\Delta\alpha} \quad .
\end{aligned} \tag{5}$$

The corresponding functions for the uu , ud , and dd diquarks, as well as for the u and d quarks are given in equation 3.

The momentum-fraction distribution function in a nucleon, in the case of N cut pomerons, is given by the following expression:

$$\begin{aligned}
&\varrho^N(x_{i_1}, x_{i_2}, \dots, x_{i_N}, x_{i_d}, x_{i_2}, \dots, x_{i_N}) = C_{i_1, i_2, \dots, i_N, i_d, \bar{i}_2, \dots, \bar{i}_N}^N \\
&\times f_{i_1}(x_{i_1}) f_{i_2}(x_{i_2}) \dots f_{i_N}(x_{i_N}) f_{i_d}(x_{i_d}) f_{\bar{i}_2}(x_{\bar{i}_2}) \dots f_{\bar{i}_N}(x_{\bar{i}_N}) \\
&\times \delta(x_{i_1} + x_{i_2} + \dots + x_{i_N} + x_{i_d} + x_{\bar{i}_2} + \dots + x_{\bar{i}_N} - 1) \quad .
\end{aligned} \tag{6}$$

This function is perfectly defined if we consider that $f_{\bar{i}}(x) = f_i(x)$. The indexes $i_j = \{u, s, d\}$ and $i_{\bar{j}} = \{\bar{u}, \bar{d}, \bar{s}\}$, $i_d = \{(uu), (ud), (dd), (us), (ds), (ss)\}$. Since we are considering nucleons as the colliding particles, the diquark can be of type (ss) only if $N \geq 3$ and of types (us) or (ds) if $N \geq 2$; we find the s-quark retardation only when $N \geq 2$.

The single-parton structure functions are obtained integrating over all other momentum fractions:

$$\begin{aligned}
\rho_{u,d}^{(N)}(x) &= C_0^{q,N} x^{-\alpha_R(0)} (1-x)^{\alpha_R(0)-2\alpha_N(0)+(N-1)2(1-\alpha_R(0))} \\
&\times [1-\gamma + \gamma(1-x)^{2\Delta\alpha}]^{N-1} \\
&= C_0^{q,N} x^{-\frac{1}{2}} (1-x)^N (1-\gamma x)^{N-1}, \quad N \geq 1 \quad . \\
\rho_s^{(N)}(x) &= C_1^{q,N} x^{-\alpha_\varphi(0)} (1-x)^{\alpha_R(0)-2\alpha_N(0)+2(N-2)(1-\alpha_R(0))+2-\alpha_R(0)-\alpha_\varphi(0)} \\
&\times [1-\gamma + \gamma(1-x)^{2\Delta\alpha}]^{N-2} \\
&= C_1^{q,N} (1-x)^{N+\frac{1}{2}} (1-\gamma x)^{N-2}, \quad N \geq 2 \quad . \\
\rho_{uu,ud,dd}^{(N)}(x) &= C_0^{qq,N} x^{\alpha_R(0)-2\alpha_N(0)} (1-x)^{-\alpha_R(0)+2(N-1)(1-\alpha_R(0))} \\
&\times [1-\gamma + \gamma(1-x)^{2\Delta\alpha}]^{N-1} \\
&= C_0^{qq,N} x(1-x)^{N-\frac{3}{2}} (1-\gamma x)^{N-1}, \quad N \geq 1 \quad . \\
\rho_{us,ds}^{(N)}(x) &= C_1^{qq,N} x^{\alpha_R(0)-2\alpha_N(0)+\Delta\alpha} (1-x)^{-\alpha_\varphi(0)+2(N-1)(1-\alpha_R(0))} \\
&\times [1-\gamma + \gamma(1-x)^{2\Delta\alpha}]^{N-2} \\
&= C_1^{qq,N} x^{\frac{3}{2}} (1-x)^{N-1} (1-\gamma x)^{N-2}, \quad N \geq 2 \quad . \\
\rho_{ss}^{(N)}(x) &= C_2^{qq,N} x^{\alpha_R(0)-2\alpha_N(0)+2\Delta\alpha} (1-x)^{-\alpha_R(0)+2(N-2)(1-\alpha_R(0))+2(1-\alpha_\varphi(0))} \\
&\times [1-\gamma + \gamma(1-x)^{2\Delta\alpha}]^{N-3} \\
&= C_2^{qq,N} x^2 (1-x)^{N-\frac{1}{2}} (1-\gamma x)^{N-3}, \quad N \geq 3 \quad .
\end{aligned} \tag{7}$$

The numerical values for the constants are $\alpha_R(0) = 0.5$, $\Delta\alpha = 0.5$ and $\alpha_N = -0.25$. The value of α_N has been chosen within the theoretically allowed range to obtain the best agreement with the proton-proton data.

The factors $[1 - \gamma + \gamma(1 - x)^{2\Delta\alpha}]^{N-J}$ in equation (7) have their origin in the fact that the s quarks take a larger portion of the nucleon momentum than the u or d quarks. It has a little effect on the structure functions when N is small. When N is large, these factors make the functions steeper at $x \rightarrow 0$.

2.2 Fragmentation Functions

The fragmentation functions are derived from Regge arguments^[37, 38]. The ones needed for the present work are listed in the appendix. I have corrected some missprints in ref. [38] and use consistently the value of α_N given above³. The constant $\lambda = 2\alpha'\bar{p}_\perp^2 \simeq 0.5$, where α' is the slope or the Regge trajectory, has been used in the expressions.

All these functions are proportional to one of the constants a_p , a_Λ , $a_{\bar{p}}$ and $a_{\bar{\Lambda}}$, which represent the universal rapidity densities of protons, Λ hyperons, antiprotons and anti- Λ hyperons respectively, around the centre-of-mass of the string. The fragmentation of a diquark into a given baryon contains two terms, one corresponds to the creation of a hadron that contains the baryon number of the diquark: primary or leading fragmentation (subindex 1), the other comes from baryon-antibaryon formation in the string: secondary fragmentation (subindex 2). Hence, the latest is proportional to the corresponding antibaryon density. Functions such as $D_{1,uu}^p(z)$, include a factor function linear with z . This is introduced to take into account the excess in the production of baryons containing the whole diquark over those that contains only one of the quarks of the diquark. Taking into account the constants that define these factors, c_0 , c_1 and c_2 , we have seven parameters with only three of them independent as a consequence of the baryon number sum rule.⁴ I have assumed that this sum rule saturates with only protons, neutrons and Λ 's as if they were the only stable baryons under strong interactions, being all the strong decays taken into account by the Regge treatment of the problem. In fact there are other hyperons that decay through electroweak processes into Λ 's and nucleons which have some contribution to the final rapidity spectra. We can easily include in the treatment these hyperons assuming that the corresponding fragmentation functions are proportional to the ones for the Λ production. This is strictly true for the cases of Σ^+ , Σ^0 and Σ^- while it is only approximate for the case of Ξ hyperons which provide a much smaller relative contribution. I take the contribution from this decays making use of the available phenomenological information. The total number of hyperons (anti-hyperons) is taken to be 1.6 the number of Λ 's ($\bar{\Lambda}$). 30% of the other strange hyperons (anti-hyperons) decay into Λ ($\bar{\Lambda}$)^[11, 43]. Hence, with all these considerations taken, we may interpret a_Λ ($a_{\bar{\Lambda}}$) as the hyperon (anti-hyperon) density in the middle of the string some of which will decay into Λ ($\bar{\Lambda}$) and others into protons (antiprotons) and neutrons (antineutrons) in equal proportions. The corrections introduced by these consideration are not significant, in the case of Λ distributions, given the accuracy of the experimental data as will be seen latter in the following sections.

³The treatment of the fragmentation functions in ref. [10] is inconsistent since two different values for α_N , -0.25 and -0.5 , were used simultaneously. This second value was also used to compute the structure functions.

⁴In ref. [10] the constraint imposed by baryon number conservation was overlooked and different values for the baryon densities in the strings were used.

The functional form of the diquark fragmentation functions for diquarks with strangeness -1 and -2 were obtained applying the results of ref. [37]. I have assumed that both strange and non-strange quarks are dynamically symmetric, hence the factor $(1+\sqrt{z})/2$. The fragmentation of a diquark into a baryon that do not contain any quark from the diquark is taken to be 0. This may be controversial since it has been suggested^[35] that an excess in the production of Ω^- over Ω^+ , in non-strange hadrons collisions, contradicts this assumption. As a matter of fact, preliminary data show a very small asymmetry in π -nucleus interactions at 500GeV/c^[39]. Nevertheless, although the data are still inconclusive, this effect, if small as it seems, may be understood in the framework of the model described in this paper: multiple collision raises the probability of having contributions to the final state coming from the fragmentation of strange diquarks that results in a net production of Ω^- .

2.3 Rapidity Distributions

We concentrate in the study of collisions between identical nuclei. The atomic weight and the atomic number are A and Z respectively. The rapidity distribution for the production of a hadron h is given by:

$$\begin{aligned} \frac{dN_{AB}^{(h)}}{dy} = & \frac{1}{\sigma_{AB}} \sum_{(n_A, n_B, n, \mu_A, \mu_B)} \sigma^{n_A, n_B, n, \mu_A, \mu_B} \{ \theta(n_B - n_A) [n_A (N_{\mu_A \mu_B}^{qq^A - q^B}(y) + N_{\mu_A \mu_B}^{q^A - qq^B}(y)) + \\ & (n_B - n_A) (N_{\mu_A \mu_B}^{\bar{q}^A - q^B}(y) + N_{\mu_A \mu_B}^{q^A - q\bar{q}^B}(y)) + (n - n_B) (N_{\mu_A \mu_B}^{q^A - \bar{q}^B}(y) + N_{\mu_A \mu_B}^{\bar{q}^A - q^B}(y))] \\ & + \text{Symmetric terms}(n_A \leftrightarrow n_B) \} \end{aligned} \quad (8)$$

In writing this expression, I neglect kinematical correlations among different strings, $N_{\mu_A \mu_B}^{a-b}$. Here, $\sigma^{n_A, n_B, n, \mu_A, \mu_B}$ is the cross-section for AB collisions where there are n inelastic nucleon-nucleon collisions involving n_A nucleons of A and n_B nucleons of B , in which at least one of the participating nucleons of A (B) suffers μ_A (μ_B) inelastic collisions.

I restrict the discussion to the case $A = B$. We can approximate equation 8, with a good degree of accuracy using average values for n_A , n_B and n .

$$\frac{dN_{AB}^{(h)}}{dy} = \bar{n}_A (N_{\bar{\mu}_A \bar{\mu}_A}^{qq^A - q^B}(y) + N_{\bar{\mu}_A \bar{\mu}_A}^{q^A - qq^B}(y)) + (\bar{n} - \bar{n}_B) (N_{\bar{\mu}_A \bar{\mu}_A}^{q^A - \bar{q}^B}(y) + N_{\bar{\mu}_A \bar{\mu}_A}^{\bar{q}^A - q^B}(y)) \quad (9)$$

Equation (9) is obtained by neglecting the dependence of the string density N on the μ 's, which are replaced by their average values $\bar{\mu}$ ⁵.

$$\begin{aligned} N_{\mu_1, \mu_2}^{a-b}(y) = & \sum_{i,j} w_N^i w_N^j \int_0^1 \int_0^1 dx_1 dx_2 \varrho_{\mu_1}^{a_i}(x_1) \varrho_{\mu_2}^{b_j}(x_2) \frac{dN^{a_i - b_j}}{dy}(y - \Delta, s_h^{a_i - b_j}) \\ & \theta(sx_1x_2 - s_h^{a_i - b_j}) \end{aligned} \quad (10)$$

Here a and b refer to quark or diquark. A sum is performed over all possible partons flavours i and j . The probability weights w^i and w^j are trivially computed from the model assumptions.

⁵In practical computations a slightly more accurate expression has been used in which the average of densities over $\mu_B = \mu_A$ were taken using the weights $\sigma_{N_A}^{\mu_A} / \sigma_{N_A}$. These weights are obtained from ref. [40]. No significant numerical difference were observed compared to the results obtained using $\bar{\mu}_A \simeq \bar{n} / \bar{n}_A$.

They depend on γ , A and Z . A mass threshold for each chain is enforced by the θ -function. Please note that this mass threshold is not always equal to the mass of hadron h since the flavour structure of the string many times forces to have other hadrons besides h in the final state. Δ is the center-of-mass rapidity of the string.

$$\frac{dN^{a_i-b_j}}{dy}(y - \Delta, s_h^{a_i-b_j}) = \begin{cases} G_{a_i}^h(y) & \text{if } y \geq \Delta \\ G_{b_j}^h(y) & \text{if } y \leq \Delta \end{cases}, \quad (11)$$

where $G(y)$ are the fragmentation functions:

$$\begin{aligned} G_{a_i}^h(y) &= Z_+ D_{a_i}^h(Z_+) \\ G_{b_j}^h(y) &= Z_- D_{b_j}^h(Z_-) \end{aligned}, \quad (12)$$

Here $Z_+ = \exp[(y - \Delta) - y_{MAX}]$ and $Z_- = \exp[-(y - \Delta) - y_{MAX}]$, y_{MAX} being the maximum rapidity that hadron h can have in the string for fixed values of momentum fractions x_1 and x_2 .

3 Proton-proton collisions

Since I have not considered sum rules others than the ones due to baryon conservation, the model leaves three free parameters that I have fixed in order to obtain the best fits to proton-proton data. At the ISR energies the structure of these collisions is very simple as we only need to consider one pomeron exchange^[7]. This makes the choice of this energy range particularly convenient as we avoid having to take into account the probability weights for the different re-scattering configurations within the same nucleon-nucleon collision. The only differences between the results of the present model and those from DPM and QGSM, at this stage, come from the choice of α_N , that was usually taken in the past to be near -0.5 .

Figure 4 represents the Feynman x distribution of protons produced in the reaction $pp \rightarrow pX$. The fit obtained agrees very well with the experimental data taken from ref. [41] particularly in the region $x_F < 0.75$. It has been pointed out that experimental points above that cut are not very reliable (see [41]) due to detector inefficiencies. The fit in the region $x \rightarrow 0$ is very sensitive to the value of α_N . For $\alpha_N = -0.5$ the results of the fit are much poorer than the one shown, which corresponds to the value of $\alpha_N = -0.25$ consistently used throughout this paper. The value of a_p fixes the values of the remaining parameters by the use of the sum rules. Figure 5 shows the fit to $pp \rightarrow \bar{p}X$. It is also worth mentioning that the same value for $a_{\bar{p}}$ was independently obtained from both fits. Please note that the computation performed do not include diffraction and, consequently, the results obtained do not show the characteristic diffraction peak at large- x .

To obtain the value of $a_{\bar{\Lambda}}$, I used the data from ref. [42] that were taken at a similar centre-of-mass energy. The reactions considered are $pp \rightarrow \Lambda X$ and $pp \rightarrow \bar{\Lambda} X$. We show the best fits in figures 6 and 7 (please mind that in this two fits only $a_{\bar{\Lambda}}$ is free, since a_{Λ} is given by the sum rules and the value of a_p) The large error bars in the experimental data do not allow for a very accurate determination of $a_{\bar{\Lambda}}$. Corrections from contributions of electroweak decays of heavier hyperons, as discussed in subsection 2.2, have also been considered. I have taken the value that best fits the data and also that is compatible with the mass suppression factor of introduced in [37].

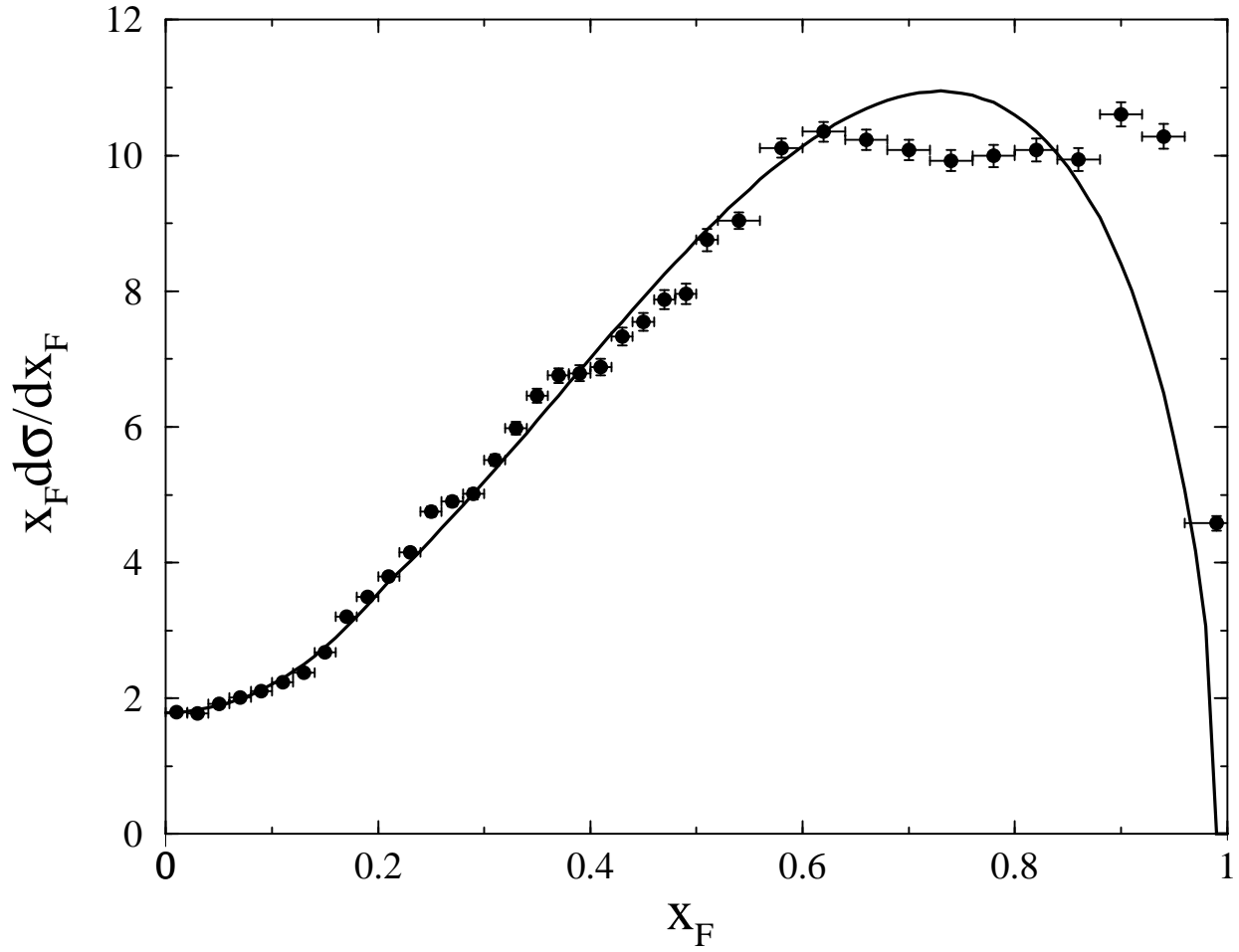


Figure 4: Fit to the Feynman x distribution of protons in the reaction $pp \rightarrow pX$. Data correspond to $p_{\text{lab}} = 400$ GeV and were taken from ref. [41].

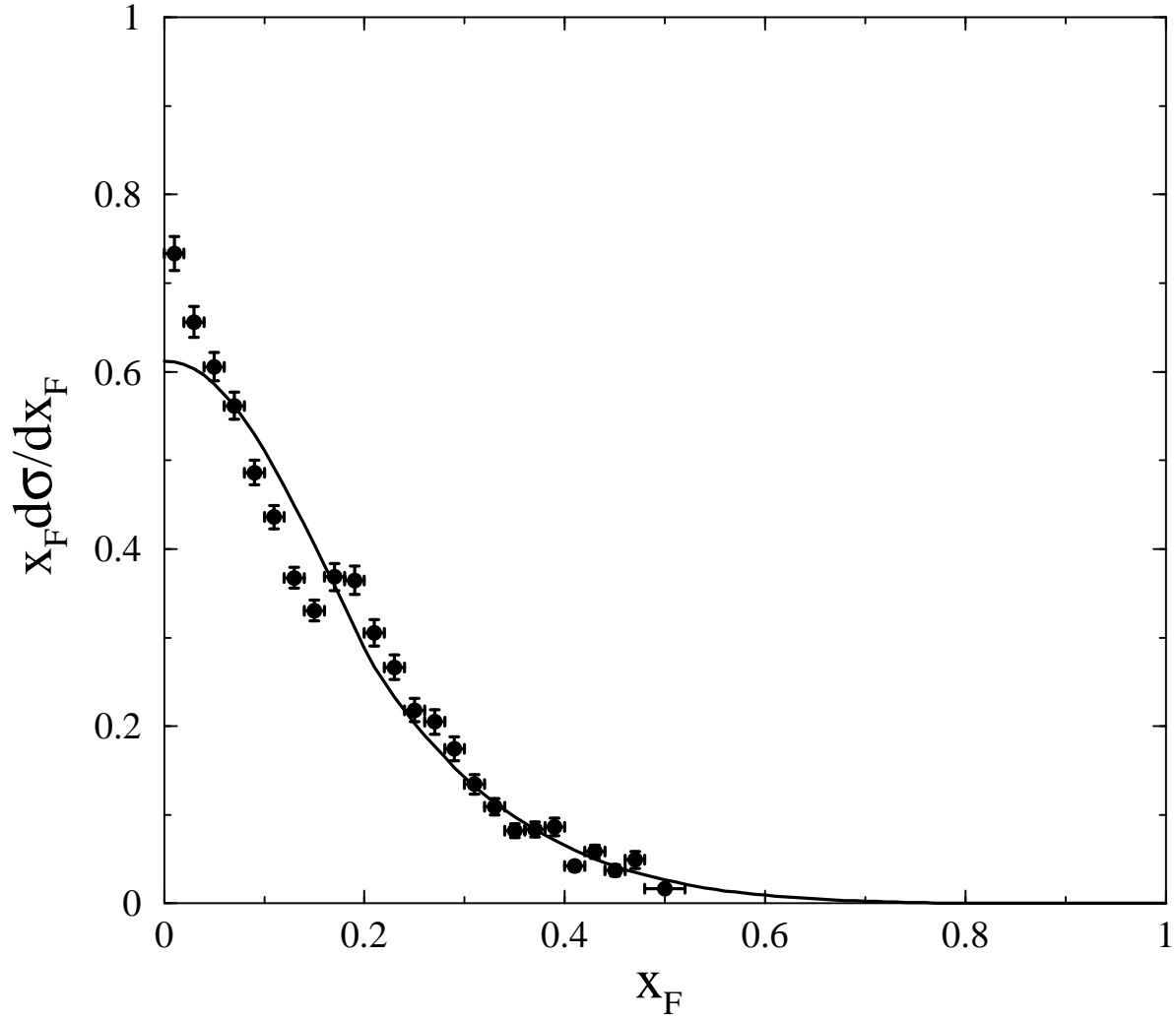


Figure 5: Fit to the Feynman x distribution of antiprotons produced in the reaction $pp \rightarrow \bar{p}X$. Data correspond to $p_{\text{lab}} = 400$ GeV and were taken from ref. [41].

The numerical values obtained are: $a_p = 0.667$, $a_\Lambda = 0.282$, $a_{\bar{p}} = 0.077$, $a_{\bar{\Lambda}} = 0.057$, $c_0 = 1.430$, $c_1 = 6.076$ and $c_2 = 67.560$.

4 Nucleus-Nucleus collisions

At this point we have a model for nucleus-nucleus collisions which contains no free parameters.

The result for the rapidity distribution of Λ hyperons produced in central sulfur-sulfur collisions is compared with the experimental data from the CERN-NA35^[11] Collaboration in figure 8. The short-dashed line corresponds to the results of the model without the sea-valence diquark symmetry introduced in this paper. As we can see, both models give similar results at $y_{CM} = 0$, while there is a remarkable difference in the fragmentation region where only the present model reproduces the data. The data points are not corrected for particles originated from electromagnetic Σ^0 ($\bar{\Sigma}^0$) decays and from weak Ξ ($\bar{\Xi}$) decay. These decays have been taken into account as described in 2.2. The uncorrected results are showed with a long-dashed line and represent the total strange hyperon distribution. In computing the correction an effective recoil, due to the decay of the resonances of 0.2 units in rapidity was introduced which has none or very little effect on the results. Figure 9 shows the agreement between the $\bar{\Lambda}$ distribution and the data points from the same experiment. Again, the dashed line corresponds to the uncorrected hyperon distribution. The only disagreement is with the point near $y_{CM} = 0$ in the Λ distribution.

Figure 10 shows the proton minus antiproton distribution in central (solid line) and peripheral (dashed-dotted line) sulfur-sulfur collisions. The data points were also taken by the CERN-NA35 collaboration^[12]. For central collisions, the agreement in the fragmentation region of the spectrum is very good while the data show an overpopulation of protons around $y_{CM} = 0$. The data were extracted from the measured charge asymmetry of the final state applying model dependent corrections. The cancellations of $p - \bar{p}$ and $\pi^+ - \pi^-$ have been assumed due to the isospin symmetry of the system. The results showed here do not make use of the first assumption above. A small difference, not significant in magnitude, is obtained in the central rapidity region when we compute the leading proton distribution as if the $p - \bar{p}$ cancellation was exact, leaving the integrated correction equal to zero as it should. From quark flavour counting the model predicts an overall $\pi^+ - \pi^-$ cancellation and an negligible change on this result due to any local effect. Corrections based on a Monte Carlo simulation (Fritiof) to the data have also been applied to estimate the $K^+ - K^-$ contribution to the charge asymmetry. The model presented here predicts a much higher production of Λ , in agreement with the data, than Fritiof whose results are very close to those of this model without the new components (dashed line fig. 8). For each extra produced lambda we are left with a \bar{s} quark at the end of one string that will appear in the final state as a K^+ or a K^0 in equal proportions. The obvious conclusion is that this model predicts a higher $K^+ - K^-$ asymmetry concentrated in the central rapidity region and whose total value is equal to one half the excess of Λ predicted by this model over the predictions of Fritiof. I have added a Gaussian correction to the $p - \bar{p}$ distribution that accounts for the missed point in the central region (dashed line). Given the long error bars, the precise shape of this correction do not matter significantly. It is interesting to notice that another correction to the Λ distribution might be necessary due to the effect on the $\Lambda \rightarrow p\pi^-$ background coming from $K^0 \rightarrow \pi^+\pi^-$. Although, there is not enough information available to

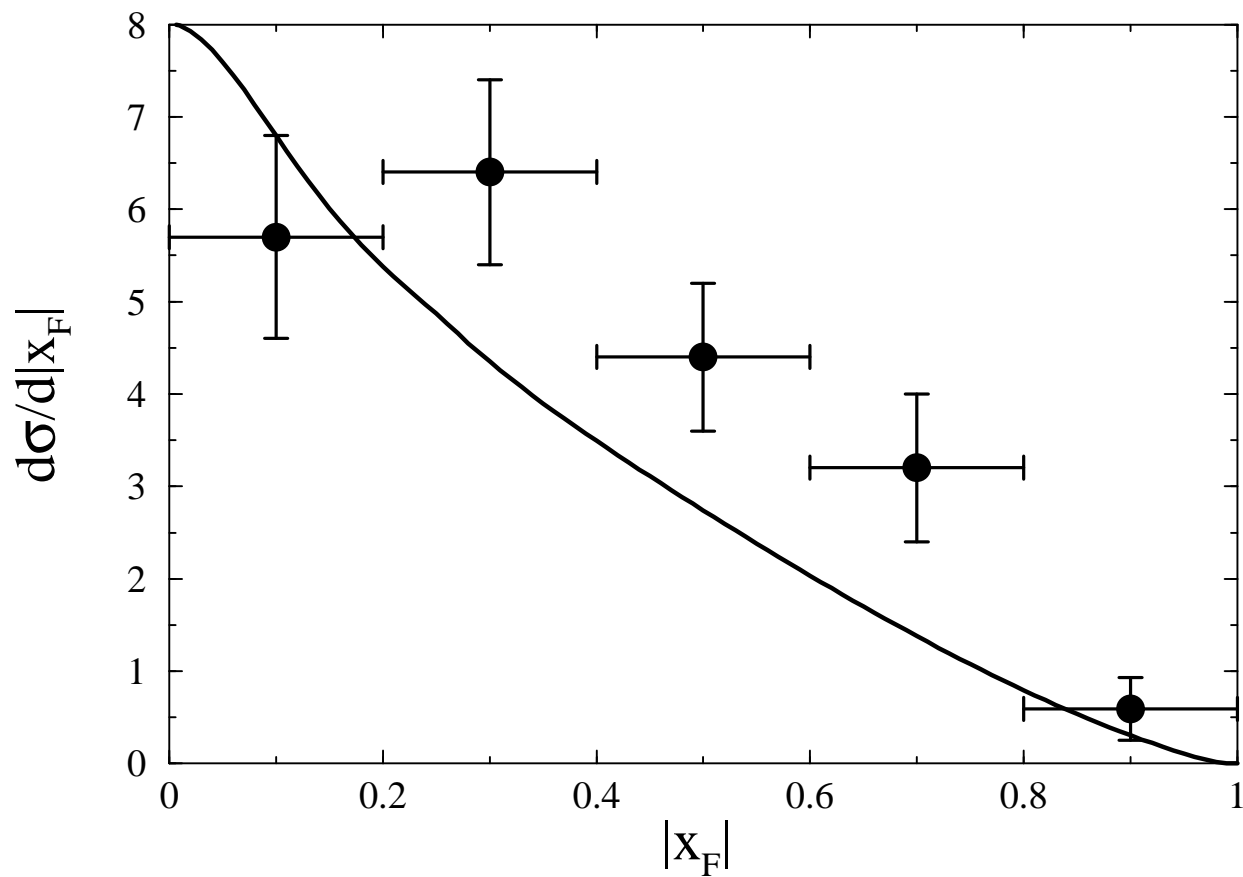


Figure 6: Fit to the Feynman x differential cross section $d\sigma/dx$ (given in mb) for the inclusive production of Λ in the reaction $pp \rightarrow \Lambda X$. Data correspond to $p_{\text{lab}} = 405$ GeV and were taken from ref. [42].

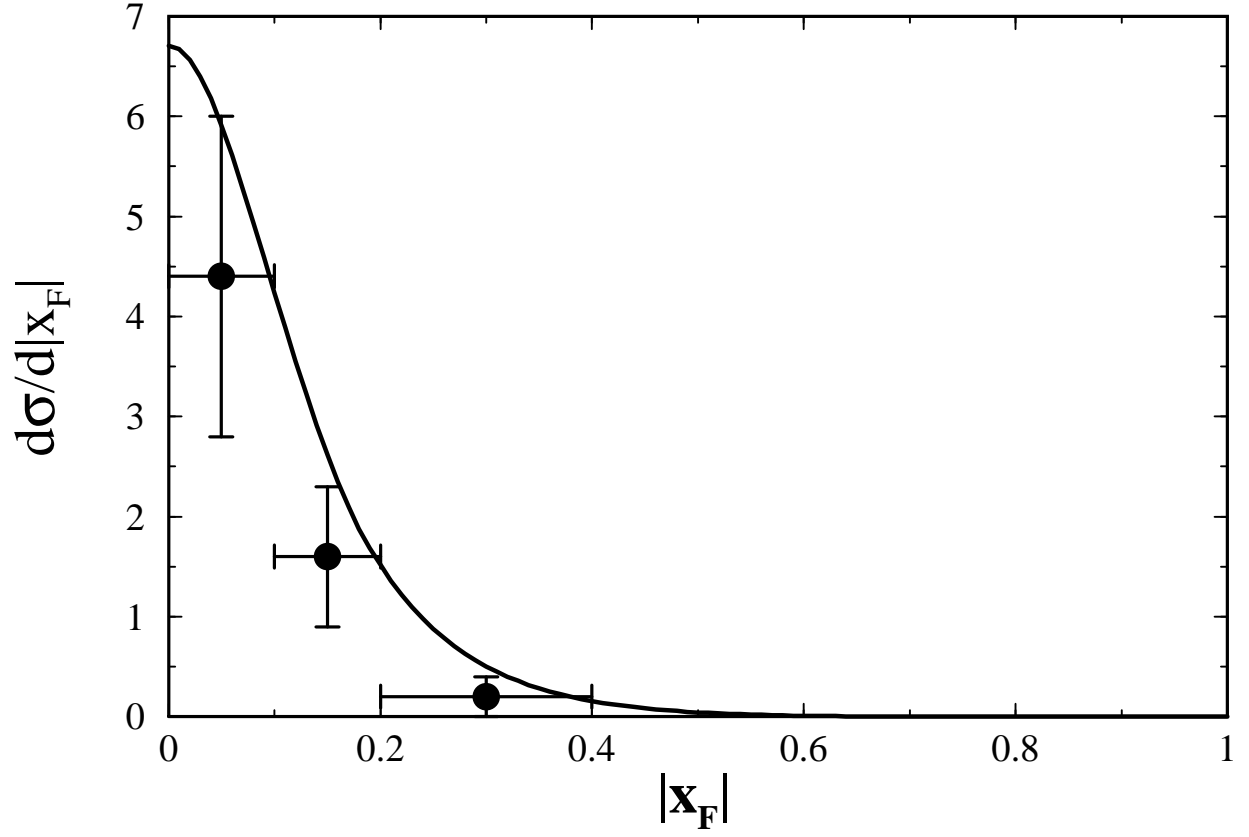


Figure 7: Fit to the Feynman x differential cross section $d\sigma/dx$ (given in mb) for the inclusive production of $\bar{\Lambda}$ in the reaction $pp \rightarrow \bar{\Lambda}X$. Data correspond to $p_{\text{lab}} = 405$ GeV and were taken from ref. [42].

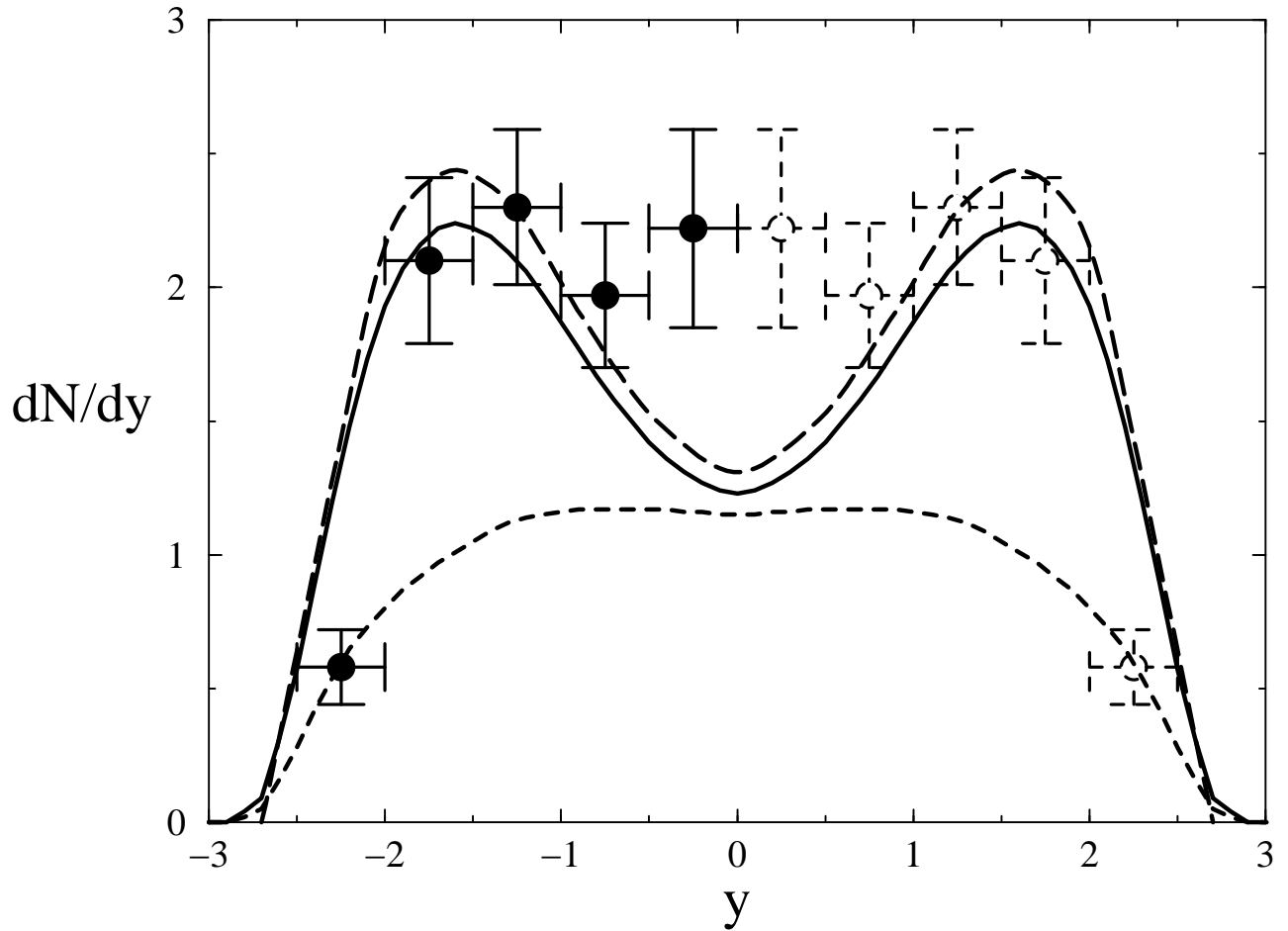


Figure 8: Rapidity distribution of Λ 's produced in central sulphur-sulphur collisions represented in the nucleon-nucleon centre-of-mass reference frame. The solid line corresponds to the results of this model while the short-dashed line are the results obtained when the new components are not included. The long-dashed line represents the total strange-hyperons spectrum. The data points are from ref.[11] and have been reflected onto positive rapidities.

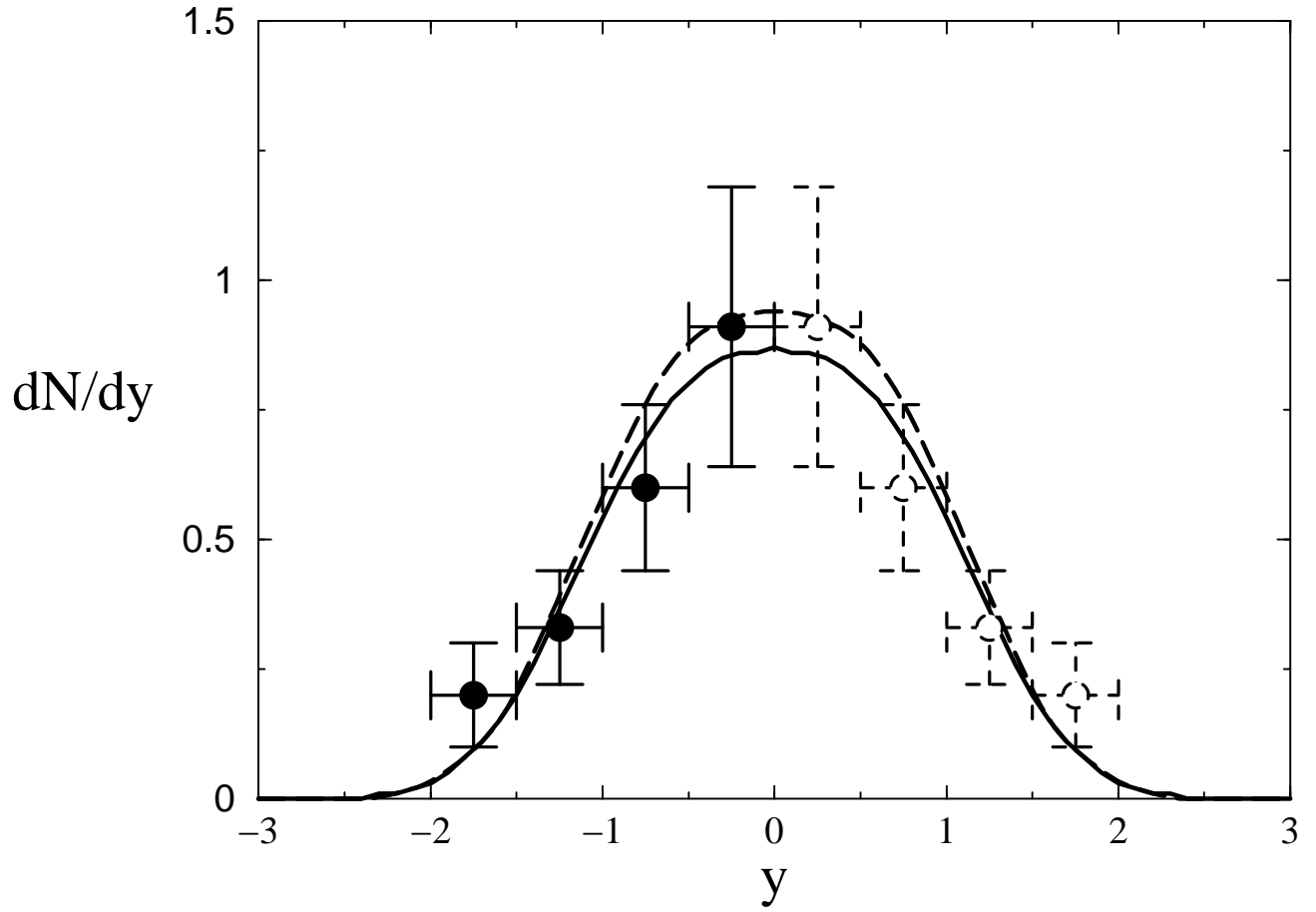


Figure 9: Rapidity distribution of $\bar{\Lambda}$'s produced in central sulphur-sulphur collisions represented in the nucleon-nucleon centre-of-mass reference frame (solid line) and the total strange hyperons spectrum (dashed line) . The data points are from ref. [11] and have been reflected onto positive rapidities.

assume that this background has not been correctly subtracted in the experimental analysis.

Figure 11 shows the predictions for the rapidity spectra of Λ and $\bar{\Lambda}$, solid lines, produced in central Pb-Pb collisions. The experimental points correspond to preliminary data from the NA49 Collaboration^[44]. The dashed lines correspond to the total hyperon (antihyperon) distributions. Figure 12 compares the result for the net proton distribution with data from the same collaboration^[43]. These data points were obtained subtracting the background due to the decays $\Lambda \rightarrow p\pi^-$ using the results of a Monte Carlo simulation. Correcting for the difference between the Λ spectrum predicted by this model and the one used in the experimental analysis, we obtain the solid line out of the net distribution (dashed-dotted line). I have also corrected for the $K^+ - K^-$ asymmetry as explained above, dashed line. As we can see, the experimental data tend to show a larger stopping in Pb-Pb collisions than what the model predicts.

As mentioned before, I have made use of the Galuber-Gribov model to obtain the average numbers of participating nucleons and nucleon-nucleon collisions. I have used the value $\sigma_{NN}^{\text{in}} = 30$ mb for the inelastic nucleon-nucleon cross section. The profile functions were obtained using the nuclear matter distribution given in ref. [45]. They consist of three parameters, individually fitted to nuclear data, functions and are more accurate than the Saxon-Wood density functions used in the past. The actual numerical values used for central S-S, $\bar{n}_A = 27.8$ and $\bar{n} = 62.8$, were obtained requiring that $b < 1$, where b is the impact parameter. For peripheral collisions we have $\bar{n}_A = 9.7$ and $\bar{n} = 14.7$, while for central Pb-Pb collisions are $\bar{n}_A = 204.4$ and $\bar{n} = 895.9$.

To perform the computations, I have taken the values of the proton and Λ transverse mass equal to 1.1 and 1.3 GeV respectively, in agreement with the data from [15].

5 Conclusions

In order to explain the data on baryon rapidity spectra presented by the NA35 collaboration, I have included into the DPM and the QGSM models components that were previously overlooked. They are compatible with the $1/N$ expansion of QCD on which these two models are based. A discussion over the right structure functions for the string's ends leads to the adoption of the ones proposed by the QGSM, as they are the only ones consistent with the model's assumptions. The fragmentation functions are obtained from the planar approximation to Regge diagrams. They have been published elsewhere except for the ones corresponding to strange diquark that are published here for the first time. All of them are given in the appendix. Once taken into account the baryon-number sum-rules, the number of free parameters of the model is reduced to 3. The numerical values of these parameters have been obtained fitting data of inclusive baryon and antibaryon production in proton-proton collisions. The sum rules allow us to obtain the fragmentation functions that do not contribute to proton-proton collisions at ISR energies.

The model has strong theoretical grounds and all the approximations done are well justified, being the uncertainties introduced by them small and well under control.

At the level of nucleus-nucleus collisions, we have a model which contains no free parameters. The $\bar{\Lambda}$ distribution for central sulphur-sulphur collisions was computed and a perfect agreement with the experimental data was obtained. This result does not depend on the new components introduced in this paper; all the $\bar{\Lambda}$ particles come from baryon-antibaryon formation in the strings, which is essentially independent of the parton components at the end of the string. This

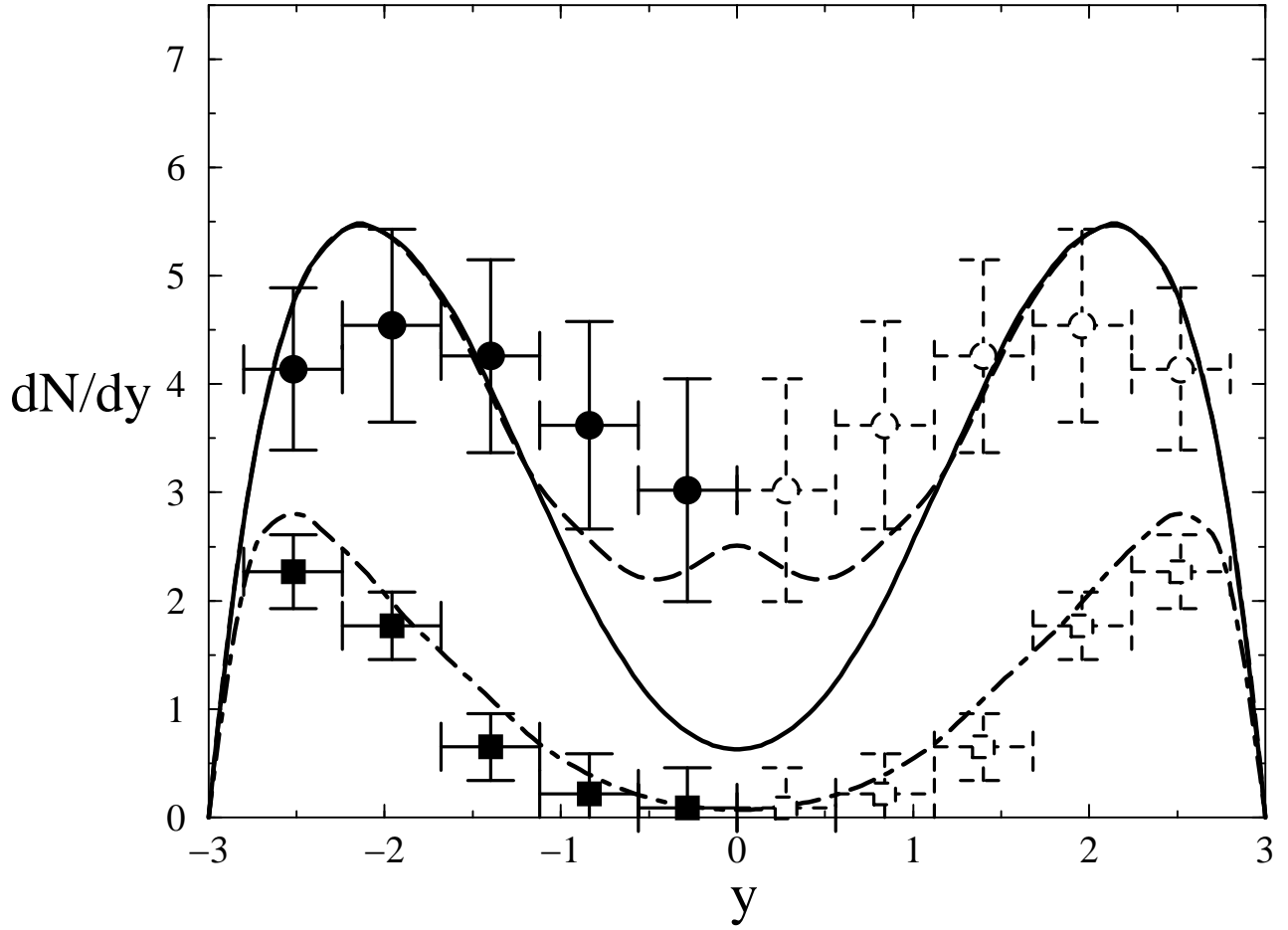


Figure 10: $p - \bar{p}$ rapidity distribution in sulphur-sulphur collisions represented in the nucleon-nucleon centre-of-mass reference frame. The dashed-dotted line corresponds to primary protons produced in peripheral collisions; the solid line are the results for the proton minus antiproton distribution in central collisions. The data points are from ref. [12] and have been reflected onto positive rapidities. The dashed line represents the correction for the excess of $K^+ - K^-$. See text for a more detailed explanation.

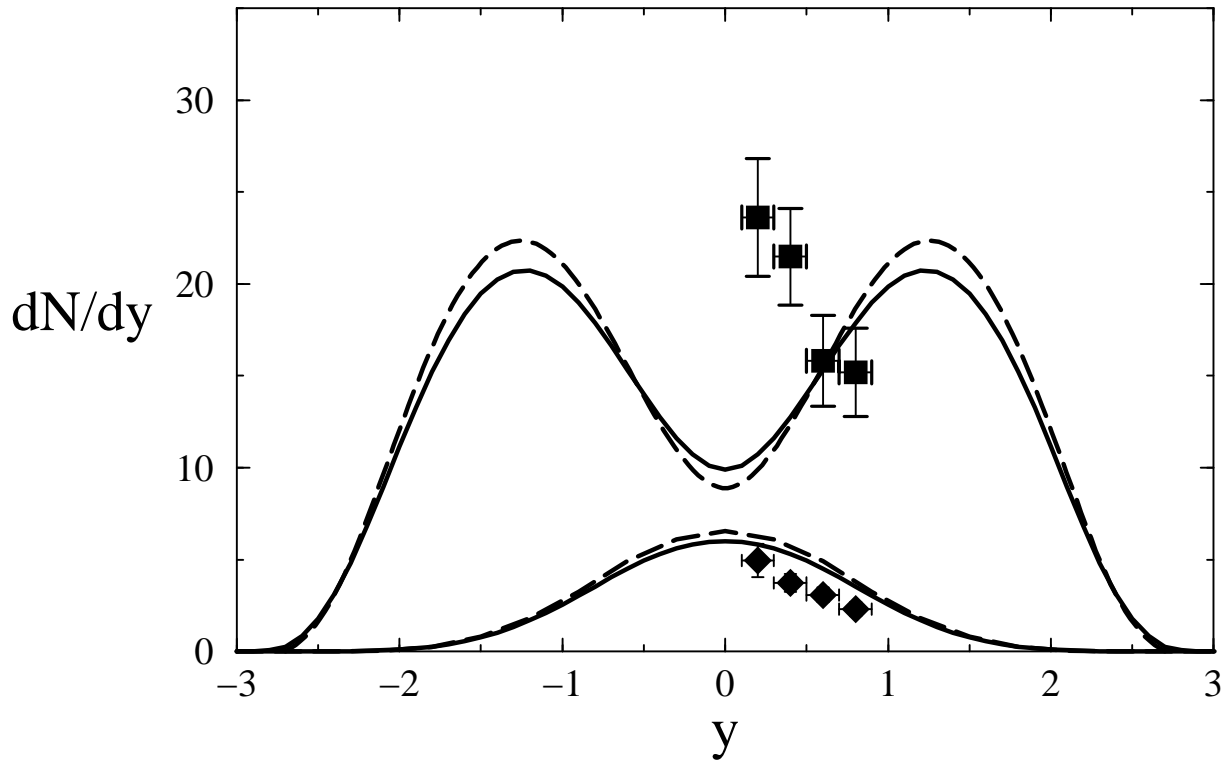


Figure 11: Rapidity distribution of Λ 's and $\bar{\Lambda}$'s, solid lines, produced in central $PbPb$ collisions represented in the nucleon-nucleon centre-of-mass reference frame. The dashed lines represent the total hyperons (anti-hyperons) distributions. Data points are from ref. [44].

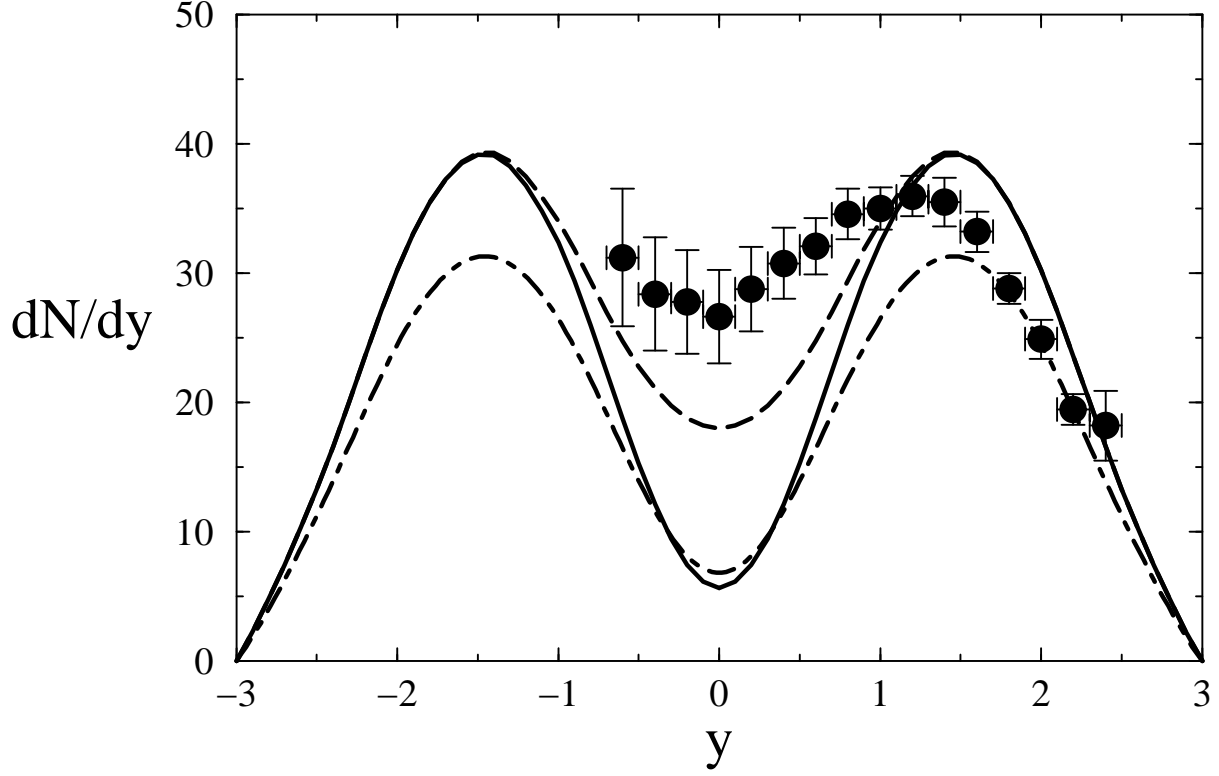


Figure 12: Rapidity $p - \bar{p}$ distribution in central $PbPb$ collisions represented in the nucleon-nucleon centre-of-mass reference frame. The solid line corresponds to the prediction including the correction from hyperon electroweak decays into protons applied to the initial proton distribution, dashed-dotted line. The dashed line represents the correction for the excess K^+ over K^- (see text for an explanation). Data points are from ref. [43].

result is very relevant since it clearly shows that the \bar{s} content at the central rapidity region is very well understood with no need to assume collective effects such as QGP formation.

I have also computed the rapidity distribution for the Λ hyperons in central sulphur-sulphur collisions and compared it with data from the same collaboration. The results show a remarkable increase of the rapidity distribution in the fragmentation region well in agreement with the experimental data. This is due to the inclusion of chains initiated by diquarks that can contain a quark from the nucleon sea. The fact that this sea-quark has a probability of being strange, obtained by independent analysis, is responsible for this effect. The only disagreement with the data is seen at the central rapidity region.

The net proton distribution for the same collisions has also been obtained and compared with data of the same collaboration. We observe a good agreement between the model results and the experimental points in the fragmentation region. Once the correction of the electric charge asymmetry due to the excess of K^+ over K^- is included, we also understand the spectrum at mid-rapidities.

The NA35 data on baryon distributions do not support that the formation of QGP has taken place or that we need to take into account collective effects of any sort. I have compare the model results with the preliminary data on Λ and $\bar{\Lambda}$ rapidity distributions in Pb-Pb collisions from the NA49 Collaboration; a partial agreement with the data was found. Unfortunately there are no points available in the fragmentation region. The comparison with the $p - \bar{p}$ spectrum measured by the same collaboration shows that the model under-predicts the stopping power in Pb-Pb collisions. This raises the interesting question about which of the model assumptions fails for the case of very heavy nuclei. It could be that effects like those of references [20] and [21] have a significant contribution to this stopping, falling within the experimental errors in the case of sulphur-sulphur collisions. This possibilities should be careful check in hadron-hadron interactions as they contain the implicit assumption that the wave function of the colliding hadron couples to the pomeron over a rapidity region larger than one unit. This may have an effect on diffractive scattering. The assumption that collisions between heavy nucleus can be decomposed as nearly uncorrelated nucleon-nucleon collisions, as implied by the use of the Galuber-Gribov model, may also fail when the size of the nuclei involved becomes very large.

Another important conclusion, that has been obtained as a byproduct, is that the analysis performed on the proton-proton data strongly support a value for the intercept of the N trajectory close to -0.25 . This is also a major result of the model that in return can help to establish a more accurate value for the mass of some resonances.

For future works it is left the detailed study of the meson sector. Also the implications of the new structure of the pomeron-hadron coupling discussed in the paper will be investigated in order to shed light on other outstanding problems such as heavy quark formation in hadronic and nuclear collisions.

Acknowledgements. I want to thank A. Capella for his continuous support and encouragement, also for pointing out a mistake in the first version of the manuscript. To him and to A. Kaidalov for discussions and many useful explanations and comments about their previous works. Also my gratitude goes to N. Armesto, S. Pepin and M. McDermott for comments and discussions and to A. Sabio-Vera for help with the technicalities

of typesetting the manuscript.

Appendix

I list here the fragmentation functions into baryons and antibaryons. The ones not shown can be obtained applying isospin symmetry $p \leftrightarrow n$, $u \leftrightarrow d$.

$$\begin{aligned}
D_{1,uu}^p &= \frac{a_p}{z} z^{2(\alpha_R(0)-\alpha_N(0))} (1-z)^{-\alpha_R(0)+\lambda} (1+c_0 z) = \frac{a_p}{z} z^{1.5} (1+c_0 z) \\
D_{1,uu}^n &= \frac{2}{3} \frac{a_p}{z} z^{2(\alpha_R(0)-\alpha_N(0))} (1-z)^{-\alpha_R(0)+\lambda+2(1-\alpha_R(0))} = \frac{2}{3} \frac{a_p}{z} z^{1.5} (1-z) \\
D_{1,uu}^\Lambda &= \frac{a_\Lambda}{z} z^{2(\alpha_R(0)-\alpha_N(0))} (1-z)^{-\alpha_R(0)+\lambda+\Delta\alpha+2(1-\alpha_R(0))} = \frac{a_\Lambda}{z} z^{1.5} (1-z)^{1.5} \\
D_{1,ud}^p &= \frac{a_p}{z} z^{2(\alpha_R(0)-\alpha_N(0))} (1-z)^{-\alpha_R(0)+\lambda} = \frac{a_p}{z} z^{1.5} = D_{1,ud}^n \\
D_{1,ud}^\Lambda &= \frac{a_\Lambda}{z} z^{2(\alpha_R(0)-\alpha_N(0))} (1-z)^{-\alpha_R(0)+\Delta\alpha+\lambda} = \frac{a_\Lambda}{z} z^{1.5} (1-z)^{0.5} \\
D_{1,dd}^p &= D_{1,uu}^n \quad , \quad D_{1,dd}^n = D_{1,uu}^p \quad , \quad D_{1,dd}^\Lambda = D_{1,uu}^\Lambda \\
D_{1,us}^p &= \frac{1}{2} \frac{a_p}{z} z^{2(\alpha_R(0)-\alpha_N(0))} (1-z)^{-\alpha_R(0)+\lambda+\Delta\alpha+2(1-\alpha_R(0))} (1+z^{\Delta\alpha}) = D_{1,us}^n \\
&= \frac{1}{2} \frac{a_p}{z} z^{1.5} (1-z)^{1.5} (1+z^{\frac{1}{2}}) \\
D_{1,us}^\Lambda &= \frac{1}{2} \frac{a_\Lambda}{z} z^{2(\alpha_R(0)-\alpha_N(0))} (1-z)^{-\alpha_R(0)+\lambda} (1+z^{\Delta\alpha}) (1+c_1 z) \\
&= \frac{1}{2} \frac{a_\Lambda}{z} z^{1.5} (1+z^{\frac{1}{2}}) (1+c_1 z) \\
D_{1,ds}^p &= D_{1,us}^p \quad , \quad D_{1,ds}^n = D_{1,us}^n \quad , \quad D_{1,ds}^\Lambda = D_{1,us}^\Lambda \quad , \quad D_{1,ss}^p = 0 \quad , \quad D_{1,ss}^n = 0 \\
D_{1,ss}^\Lambda &= \frac{a_\Lambda}{z} z^{2(\alpha_R(0)-\alpha_N(0))+\Delta\alpha} (1-z)^{-\alpha_R(0)+\lambda+\Delta\alpha+2(1-\alpha_R(0))} (1+c_2 z) \\
&= \frac{a_\Lambda}{z} z^2 (1-z)^2 (1+c_2 z) \\
D_{2,uu}^{p,n} &= D_{2,ud}^{p,n} = D_{2,dd}^{p,n} = \frac{a_{\bar{p}}}{z} (1-z)^{-\alpha_R(0)+\lambda+4(1-\alpha_N(0))} = \frac{a_{\bar{p}}}{z} (1-z)^5 \\
D_{2,uu}^\Lambda &= D_{2,ud}^\Lambda = D_{2,dd}^\Lambda = \frac{a_{\bar{\Lambda}}}{z} (1-z)^{-\alpha_R(0)+\lambda+\Delta\alpha+4(1-\alpha_N(0))} = \frac{a_{\bar{\Lambda}}}{z} (1-z)^{5.5} \\
D_{2,us}^{p,n} &= D_{2,ds}^{p,n} = \frac{a_{\bar{p}}}{z} (1-z)^{-\alpha_R(0)+\lambda+\Delta\alpha+4(1-\alpha_N(0))} = \frac{a_{\bar{p}}}{z} (1-z)^{5.5} \\
D_{2,us}^\Lambda &= D_{2,ds}^\Lambda = \frac{a_{\bar{\Lambda}}}{z} (1-z)^{-\alpha_R(0)+\lambda+2\Delta\alpha+4(1-\alpha_N(0))} = \frac{a_{\bar{\Lambda}}}{z} (1-z)^6 \\
D_{2,ss}^{p,n} &= \frac{a_{\bar{p}}}{z} (1-z)^{-\alpha_R(0)+\lambda+2\Delta\alpha+4(1-\alpha_N(0))} = \frac{a_{\bar{p}}}{z} (1-z)^6 \\
D_{2,ss}^\Lambda &= \frac{a_{\bar{\Lambda}}}{z} (1-z)^{-\alpha_R(0)+\lambda+3\Delta\alpha+4(1-\alpha_N(0))} = \frac{a_{\bar{\Lambda}}}{z} (1-z)^{6.5} \\
D_u^p &= D_d^n = \frac{a_{\bar{p}}}{z} (1-z)^{\alpha_R(0)-2\alpha_N(0)+\lambda} = \frac{a_{\bar{p}}}{z} (1-z)^{1.5}
\end{aligned}$$

$$\begin{aligned}
D_u^\Lambda &= D_d^\Lambda = \frac{a_{\bar{\Lambda}}}{z}(1-z)^{\alpha_R(0)-2\alpha_N(0)+\lambda+\Delta\alpha} = \frac{a_{\bar{\Lambda}}}{z}(1-z)^2 \\
D_d^p &= D_u^n = \frac{a_{\bar{p}}}{z}(1-z)^{\alpha_R(0)-2\alpha_N(0)+\lambda}\left(\frac{1}{3} + \frac{2}{3}(1-z)\right) = \frac{a_{\bar{p}}}{z}(1-z)^{1.5}\left(\frac{1}{3} + \frac{2}{3}(1-z)\right) \\
D_s^{p,n} &= \frac{a_{\bar{p}}}{z}(1-z)^{\alpha_R(0)-2\alpha_N(0)+\lambda+2(1-\alpha_R(0))+\Delta\alpha} = \frac{a_{\bar{p}}}{z}(1-z)^3 \\
D_s^\Lambda &= \frac{a_{\bar{\Lambda}}}{z}(1-z)^{\alpha_R(0)-2\alpha_N(0)+\lambda} = \frac{a_{\bar{\Lambda}}}{z}(1-z)^{1.5} \\
D_{uu}^{\bar{p},\bar{n}} &= D_{ud}^{\bar{p},\bar{n}} = D_{dd}^{\bar{p},\bar{n}} = \frac{a_{\bar{p}}}{z}(1-z)^{\alpha_R(0)-2\alpha_N(0)+\lambda+2(1-\alpha_N(0))} = \frac{a_{\bar{p}}}{z}(1-z)^4 \\
D_{uu}^{\bar{\Lambda}} &= D_{ud}^{\bar{\Lambda}} = D_{dd}^{\bar{\Lambda}} = \frac{a_{\bar{\Lambda}}}{z}(1-z)^{\alpha_R(0)-2\alpha_N(0)+\lambda+\Delta\alpha+2(1-\alpha_N(0))} = \frac{a_{\bar{\Lambda}}}{z}(1-z)^{4.5} \\
D_{us}^{\bar{p},\bar{n}} &= D_{ds}^{\bar{p},\bar{n}} = \frac{a_{\bar{p}}}{z}(1-z)^{\alpha_R(0)-2\alpha_N(0)+\lambda+\Delta\alpha+2(1-\alpha_N(0))} = \frac{a_{\bar{p}}}{z}(1-z)^{4.5} \\
D_{us}^{\bar{\Lambda}} &= D_{ds}^{\bar{\Lambda}} = \frac{a_{\bar{\Lambda}}}{z}(1-z)^{\alpha_R(0)-2\alpha_N(0)+\lambda+2\Delta\alpha+2(1-\alpha_N(0))} = \frac{a_{\bar{\Lambda}}}{z}(1-z)^5 \\
D_{ss}^{\bar{p},\bar{n}} &= \frac{a_{\bar{p}}}{z}(1-z)^{\alpha_R(0)-2\alpha_N(0)+\lambda+2\Delta\alpha+2(1-\alpha_N(0))} = \frac{a_{\bar{p}}}{z}(1-z)^5 \\
D_{ss}^{\bar{\Lambda}} &= \frac{a_{\bar{\Lambda}}}{z}(1-z)^{\alpha_R(0)-2\alpha_N(0)+\lambda+3\Delta\alpha+2(1-\alpha_N(0))} = \frac{a_{\bar{\Lambda}}}{z}(1-z)^{5.5} \\
D_u^{\bar{p},\bar{n}} &= D_d^{\bar{p},\bar{n}} = \frac{a_{\bar{p}}}{z}(1-z)^{-\alpha_R(0)+\lambda+2(1-\alpha_N(0))} = \frac{a_{\bar{p}}}{z}(1-z)^{2.5} \\
D_u^{\bar{\Lambda}} &= \frac{a_{\bar{\Lambda}}}{z}(1-z)^{-\alpha_R(0)+\lambda+\Delta\alpha+2(1-\alpha_N(0))} = \frac{a_{\bar{\Lambda}}}{z}(1-z)^3 \\
D_s^{\bar{p},\bar{n}} &= \frac{a_{\bar{p}}}{z}(1-z)^{-\alpha_R(0)+\lambda+\Delta\alpha+2(1-\alpha_N(0))} = \frac{a_{\bar{p}}}{z}(1-z)^3 \\
D_s^{\bar{\Lambda}} &= \frac{a_{\bar{\Lambda}}}{z}(1-z)^{-\alpha_R(0)+\lambda+2\Delta\alpha+2(1-\alpha_N(0))} = \frac{a_{\bar{\Lambda}}}{z}(1-z)^{3.5}
\end{aligned}$$

References

- [1] J. C. Collins and M. Perry, Phys. Lett. **B34**, 1353 (1975).
- [2] A. M. Polyakov, Phys. Lett. **B72**, 224 (1977).
- [3] S. A. Bass, M. Gyulassy, H. Stöcker, and W. Greiner, INT preprint DOE/ER/40561-11-INT98, hep-ph/9810281 (1998).
- [4] J. Rafelski, Phys. Rep. **88**, 331 (1982).
- [5] B. M. P. Koch and J. Rafelski, Phys. Rep. **142**, 167 (1986).
- [6] M. Gyulassy and W. Greiner, Ann. Phys. **109**, 485 (1977).
- [7] A. Capella, U. Sukhatme, C. I. Tan, and J. T. T. Van, Phys. Rep. **236**, 225 (1994).
- [8] A. Kaidalov, Phys. Lett. **B116**, 459 (1982).
- [9] A. Kaidalov and K. A. Ter-Martirosyan, Phys. Lett. **B117**, 247 (1982).
- [10] A. Capella *et al.*, Z. Phys. C **70**, 507 (1996).

- [11] N. C. T. Alber *et al.*, Z. Phys. C. **64**, 195 (1994).
- [12] N. C. H. Ströbele *et al.*, Nuc. Phys. **A525**, 59c (1991).
- [13] J. D. Bjorken, Phys. Rev. **D27**, 140 (1983).
- [14] E. C. N. N. Biswas, in *Proceedings of the XXI International Symposium on Multiparticle Dynamics* (World Scientific, Singapore, 1992).
- [15] E. C. T. Alexopoulos *et al.*, Phys. Rev. **D46**, 2773 (1992).
- [16] H. J. Möhring, J. Ranft, A. Capella, and J. T. T. Van, Phys. Rev. **D47**, 4146 (1993).
- [17] J. Ranft, A. Capella, and J. T. T. Van, Phys Lett. **B320**, 346 (1994).
- [18] A. Capella, Phys. Lett. **B364**, 175 (1995).
- [19] N. Armesto *et al.* **B344**, 301 (1995).
- [20] A. Capella and B. Z. Kopeliovich, Phys. Lett. **B381**, 325 (1996).
- [21] D. Kharzeev, Phys. Lett. **B378**, 238 (1996).
- [22] B. Andersson, G. Gustafson, and B. Nilsson-Almquist, Nucl. Phys. **B281**, 289 (1987).
- [23] C. Hong-Mo *et al.*, Nucl. Phys. **B86**, 470 (1975).
- [24] C. Hong-Mo *et al.*, Nucl. Phys. **B93**, 13 (1975).
- [25] G. F. Chew and C. Rosenzweig, Nucl. Phys. **B104**, 290 (1976).
- [26] G. F. Chew and C. Rosenzweig, Phys. Rep. **41C**, 263 (1978).
- [27] G. F. Chew *et al.*, in *GeV and TeV Hexons from a Topological Viewpoint*, edited by J. T. T. Van (Editions Frontiers, France, 1988).
- [28] G. Veneziano, Nucl. Phys. **B74**, 365 (1974).
- [29] G. 't Hooft, Nucl. Phys. **B72**, 461 (1974).
- [30] E. Witten, Nucl. Phys. **B160**, 57 (1979).
- [31] S. Coleman, in *Pointlike Structure Inside and Outside Hadrons, Erice Lectures*, edited by A. Zichichi (Plenum, New York, 1974), p. 11.
- [32] A. Martin, W. Stirling, and R. Roberts, Phys.Rev. **D50**, 6734 (1994).
- [33] A. Bazarko *et al.*, Z.Phys.C **65**, 189 (1995).
- [34] J. A. Casado, Phys. Lett. **B309**, 431 (1993).
- [35] A. Kaidalov, personal communication.

- [36] A. Capella, A. Kaidalov, C. Merino, and J. T. T. Van, Phys. Lett. **B343**, 403 (1995).
- [37] A. B. Kaidalov, Sov. J. Nucl. Phys. **45**, 902 (1987).
- [38] A. B. Kaidalov and O. I. Piskunova, Z. Phys. C **30**, 154 (1986).
- [39] J. Solano, J. Magnin, and F. R. A. Simao, hep-ex/9710033 (1997), presented at the *5th International Conference on Relativistic Aspects of Nuclear Physics*, 27-29 Aug 1997, Rio de Janeiro, Brazil.
- [40] A. Capella *et al.*, Z. Phys. C **33**, 541 (1987).
- [41] M. Aguilar-Benitez *et al.*, Z. Phys. C **50**, 405 (1991), the data points shown in this paper were provided to the Durham Reaction Data Database by one of the authors (Y.V.Fisyak).
- [42] H. Kichimi *et al.*, Phys. Lett. **B72**, 411 (1978).
- [43] H. Appelshäuser *et al.*, nucl-ex/9810014.
- [44] T. Alber *et al.*, Presented in *Strangeness in Quark Matter 1997*.
- [45] C. W. de Jager, H. de Vries and C. de Vries, *Atomic Data and Nuclear Data Tables* 14, 479 (1974). The author is grateful to N. Armesto for generously providing the code for the computation of the nuclear profile functions.